IRAQI Academic Scientific Journals

SAMARRA JOURNAL OF ENGINEERING SCIENCE AND RESEARCH

S.J.E.S.R

Analysis of non-prismatic concrete beams under pure torsion: Numerical study

Omer F. Ibraheem [1*], Safa A. Rasheed [1]

1- Department of Civil Engineering, College of Engineering, Tikrit University, Tikrit, Iraq

Article Information

Received: 27/9/2025
Accepted: 19/1/2026

Keywords:

Non-prismatic beam, Torsion, reinforced concrete, Finite elements.

***Corresponding Author**

E-mail:
omer.f.ibrahim@tu.edu.iq

Abstract

Reinforced concrete non-prismatic beams are widely used in structural engineering. Reinforced concrete non-prismatic beams are preferred members for many applications due to their important advantages. These include bridge pier caps, long-span girder bridge, and building frames. Light weight is the major benefits of this form of the beam which allows a bigger span in comparison to prismatic members. Despite of these advantages, there are no specific recommendations provided by different codes that would insure the detailing of these elements. Members with significant torsion require complicated 3D stress analysis, particularly after the members have developed a few cracks in the earlier stages of loading leading to development of nonlinear and complicated response for the members. In the present study, a 3D analysis using finite element method has been made to study the behaviour of non-prismatic reinforced concrete beams under pure torsion. Validation of a results obtained by finite element was done through a comparison with experimental data with respect to cracking load, maximum load, and torque-twist curve. Longitudinal torsional reinforcement improves maximum capacity by about 28.6%. An increase in tapering angle by about 100% modified the torsional capacity by about 15%. Generally, the FE results matched experimental results within 8%.

1. Introduction

Reinforced concrete non-prismatic beams have been adopted in many infrastructures such as building frames, bridge piers, and portal frames. Light weight of structure, larger span that can be used in comparison to prismatic members can be attributed to the increased interesting by these members. The main disadvantages noted for these beams are specialized framework and skilled workers to construct the Molds. However, despite these advantages, very few experimental and numerical studies have investigated the response of these beams under different loading conditions. Most of the important research on non-prismatic reinforced concrete beams has focused mainly on their behaviour under shear forces. However, the shear and torsion stresses both have same actions, create diagonal tension, and have same reinforcement pattern. The studies on non-prismatic members have primarily examined the

effect of the stirrup ratio on beam capacity [1,2]. Previous research on non-prismatic reinforced concrete beams has highlighted several important parameters influencing their behaviour. Shuo et al. [1] concluded that increasing the stirrup ratio does not necessarily enhance the shear capacity of non-prismatic beams; instead, the improvement depends strongly on the tapering angle. In addition, Hou et al. [3] reported that the shear span significantly affects both the load-carrying capacity and cracking pattern, particularly in specimens without transverse reinforcement. Several studies have also demonstrated that the tapering angle has a pronounced effect on the shear strength of non-prismatic beams [4, 5, 6, 7]. Moreover, compressive strength has been identified as a crucial parameter influencing shear capacity, as observed by Rauf and Ramadhan [8]. A statistical assessment of the experimental data available in the literature was later presented by Rauf and Ramadhan [9] and Karrar et al. [10], providing a broader understanding of governing parameters.

In the numerical and analytical domain, Godínez-Domínguez et al. [11] proposed a simplified finite element (FE) model using SAP2000 to develop a nonlinear static representation of eight hunched beams failing in shear. Their model indirectly incorporated both longitudinal and transverse reinforcement within the concrete continuum. This work paved the way for further numerical investigations. Subsequent finite element studies, such as those by Shuo et al. [1] and Al-Ahmed et al. [5], successfully simulated the behaviour of non-prismatic beams under shear loading, achieving strong agreement with experimental results.

Jaafer and Abdulghani [12] studied the response of non-prismatic beams by nonlinear finite element model. Fifteen specimens were modelled and analysed under flexural and shear control loading. A good agreement was noticed between the model and experimental results.

However, all the above-mentioned researches investigated the general behaviour of non-prismatic beams under shear loading. Jebur [13], studied the behaviour of reinforced concrete non-prismatic beams using FEM to describe the response of these elements under pure torsion. Ten specimens (with and without reinforcement) were studied at various tapering angles. Although the results were verified firstly with the experimental data presented by Tena-Colunga et al. [4] on specimens under shear loading, it can be represented as one of the earlier studies on the response of non-prismatic beams under pure torsion.

Few studies have investigated the torsional behaviour of non-prismatic concrete beams using validated 3D finite element models, and this work aims to address that gap. In the present study, the overall behaviour of non-prismatic concrete beams is examined using a nonlinear finite element model developed in the ANSYS commercial software. The numerical results are verified against available experimental data and subsequently discussed.

2. Experimental study

The experimental study includes eight non-prismatic beams sorted according to the tapering angle into two main groups. All specimens have a constant length and width of 1500 mm and 150 mm, respectively. The depth was varied from 150 mm to 300 mm according to the tapering angle as shown in Fig. 1.

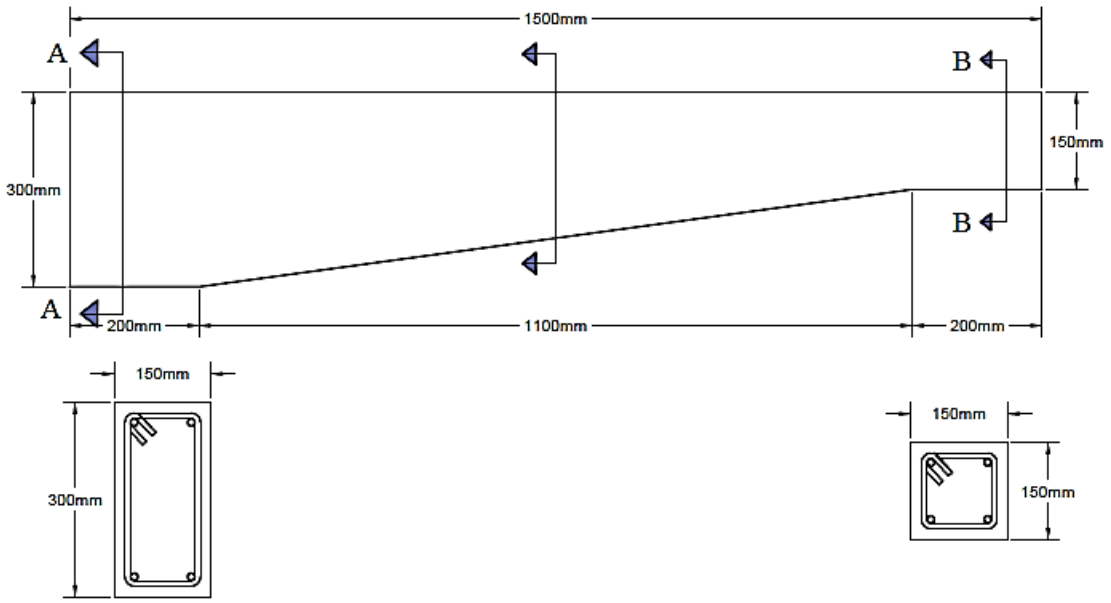

Fig. 1. Specimens' layout.

The non-prismatic beams were designed according to the specifications of the ACI-code 318M-19 [14], and the details of beam reinforcement are shown in Fig. 1. The stirrup reinforcement spacing was changed along the beam length according to ACI-Code requirements.

Longitudinal reinforcement is present in all specimens, with 2ϕ12 mm in each corner. Moreover, ϕ8 mm and ϕ10 mm steel deformed bars spaced at different spacings offer as torsional reinforcement [15]. The longitudinal torsional reinforcement at mid-depth of the specimens was chosen as parameter adopted with two different diameters. The main parameters investigated were:

1.Tapering angle (α) (3.88°, and 7.765°)

2. Stirrups area.

3.Longitudinal torsional reinforcement.

Table 1 list the main parameters and the specimens subscript.

The subscripts of the specimens were: Beam, larger beam depth, stirrup diameter, and torsional reinforcement. For example: B300-8-L, means a non-prismatic beam of 300 mm depth reinforced by 8 mm stirrups and longitudinal torsional reinforcement. Table 2 summarizes the important results collected.

Table 1. The specimens and parameters investigated.

Beam No.	Tapering angle (deg)	Torsional long. Reinf	Stirrups area
B300-8-L	7.765	2 ϕ 8	ϕ 8
B300-8	7.765	-	ϕ 8
B300-10-L	7.765	2 ϕ 8	ϕ 10
B300-10	7.765	-	ϕ 10
B225-8-L	3.88	2 ϕ 8	ϕ 8
B225-8	3.88	-	ϕ 8
B225-10-L	3.88	2 ϕ 8	ϕ 10
B225-10	3.88	-	ϕ 10

2.1 Materials

Ordinary Portland cement was used in the design of the concrete mix and a target strength was specified to 25 MPa in 28 days. The concrete mixture was made of cement, sand, and aggregate, with mix proportion of (1:1.8:3.6), a water-to-cement ratio of (0.457) was dependent in the present mix [16]. The average compressive strength of three standard cubes 150×150×150 mm for the concrete mix was 28.4 MPa at 28 days, while the average split tensile strength was 3.3 MPa. Tensile tests were carried out on steel bars adopted in the present study in the laboratory, according to ASTM - A615 [17]. Table 2 describes yield stress and ultimate strength for steel bars.

Table 2. Characteristics of steel reinforcement bars.

Bar Diameter (mm)	Yield stress Fy (MPa)	Ultimate stress Fu (MPa)	Elongation %
8	442	589	11.2
10	535	626	9.41
12	576	665	12.7

2.2 Test setup

The structural loading frame shown in Fig. 2 was designed to apply a pure torsional loading on tested specimen.

A load cell was used to record the magnitude of the applied load while the developed deformation detected by Linear Variable Differential Transformer (LVDT).

The torsional arm was created by firmly attaching steel frames to the ends of beam specimens. It featured a lever arm that was 200 mm and measured from the centre of the steel shaft to the edge of the terminal. All specimens had their maximum twisted moment (torque) and resistance to cracking evaluated with the help of a hydraulic jack and an electric motor, each capable of delivering a maximum load of 250 kN at a loading rate of 0.064 kN/sec. The torsional arm was loaded with a standard load using a hydraulic jack, and the load was applied to a dish-serrated steel shaft, which led to the generation of twisting torque.

Fig. 2. Specimen and Test machine.

3. Finite element model

3.1 Geometry

In the experiments, stirrups were placed closer to the beam ends to ensure failure in the middle section. In FE, this property can be adopted to avoid local failure at beam ends due to stress concentration. The end parts were strengthened by steel plates to be within the elastic range when the couple load is applied at the free end of the beam. The layout of the FE model of non-prismatic beam is shown in Fig. 3.

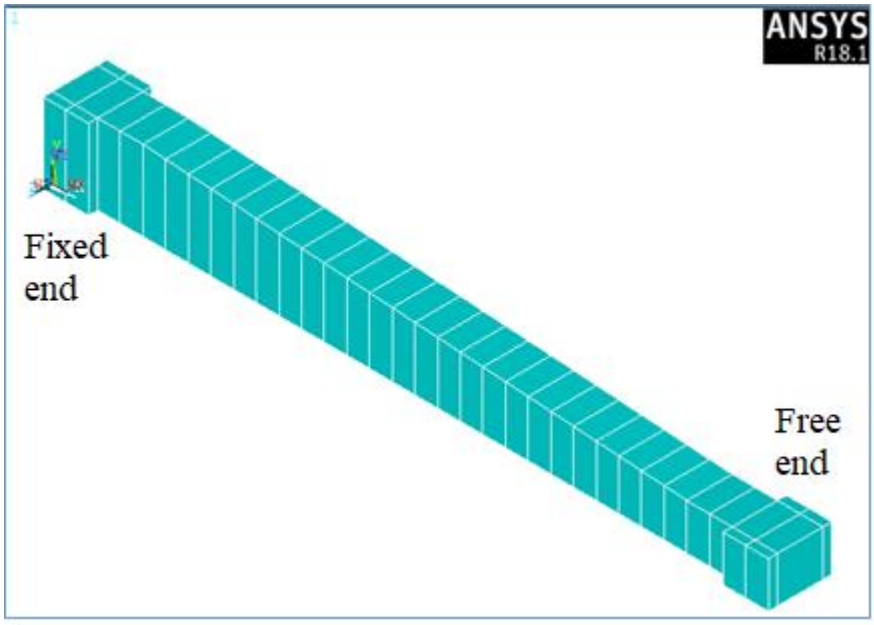

Fig. 3. Beam's FE geometry.

3.2 Boundary conditions

A significant role played by the boundary conditions in FE modelling. There are two boundary conditions used in the present model. The FE model was fixed at one end of beam and held at the other end to rotate about x –axis as shown in Fig. 4.

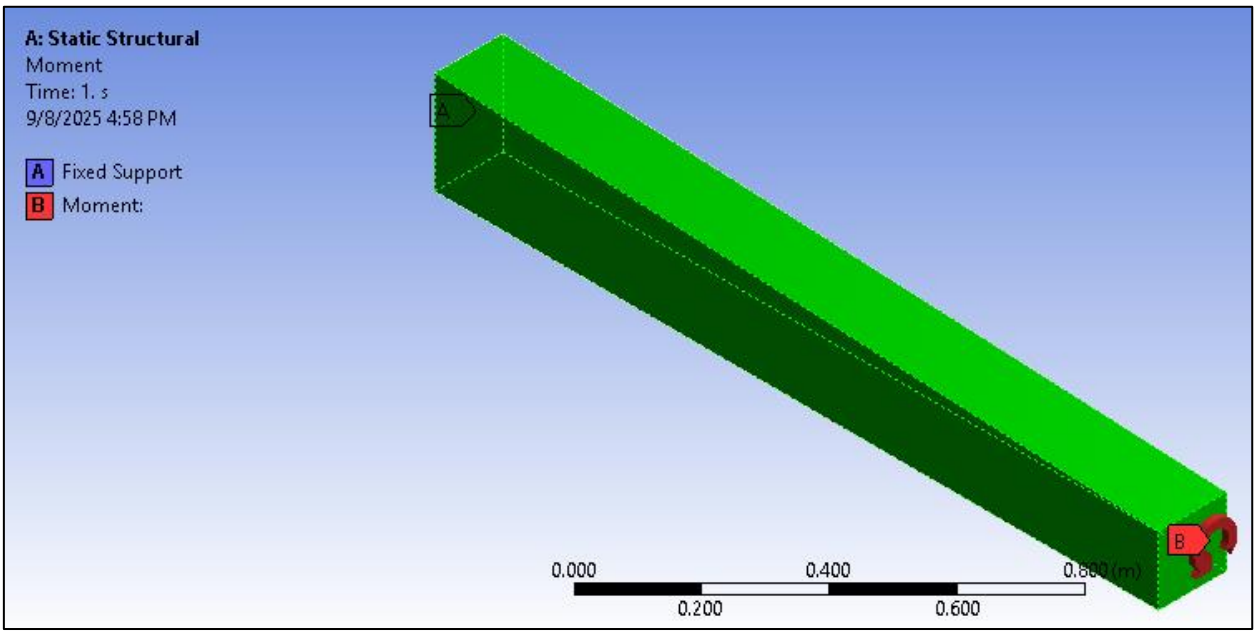

Fig. 4. Beam's boundary conditions.

3.3 Element types

Concrete and reinforced steel are represented by separate material models, which are combined together to model the behaviour of composite reinforced concrete material. Concrete was modelled with an 8-node isoperimetric 3D solid brick element (SOLID65), and the discrete reinforcement bar was modelled as 2-node separate truss element (3D Link8) [18]. These two elements were capable of describing and modelling the nonlinear response of reinforced concrete.

3.4 Material modelling

Concrete is assumed as linear behaviour before cracking and has nonlinear behaviour after cracking. Compressive and tensile strength of concrete were taken from the experimental data. Poisson's ratio was assumed to be 0.2 and the modulus of elasticity was adopted from ACI-code 318M-19 [14]. Crushing is assumed to occur when the total strain reaches the limit value. In the present study, a multilinear stress-strain curve is used for the uniaxial stress-strain relationship beyond the limit of elasticity as shown in Fig. 5. The work-hardening stage of behaviour was modelled and a perfectly plastic response is assumed to occur when the peak compressive stress is reached.

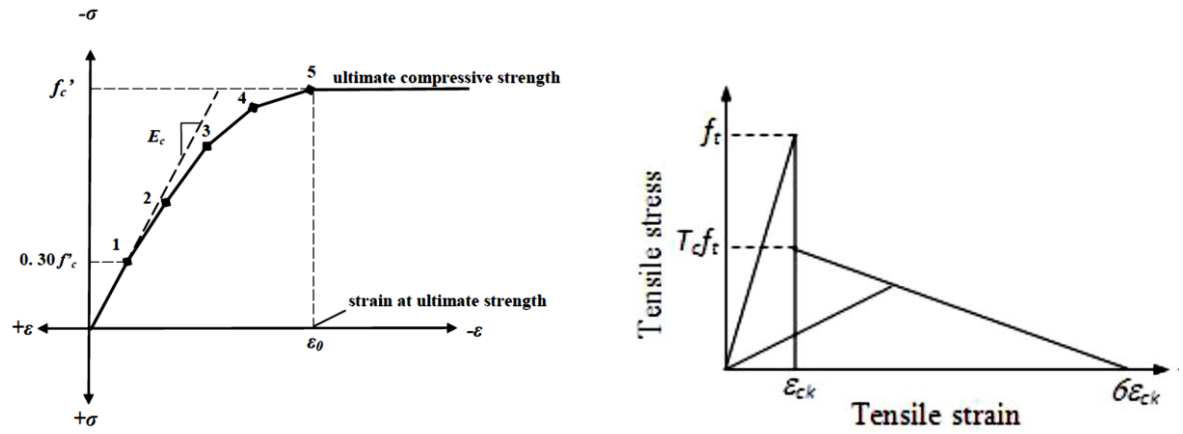

(a) Compression (b) Tension

Fig. 5. Stress-strain model for concrete (a) Compression (b) Tension [19].

Concrete is a brittle material, so the tensile strength was modelled to drop to zero when cracking occurs, see Fig. 5. When tensile strength exceeds, all the tensile strength will be carried by steel bars [18].

Bilinear Isotropic Hardening was adopted to model the stress-strain relationship of steel material in tension and compression as shown in Fig. 6 [18].

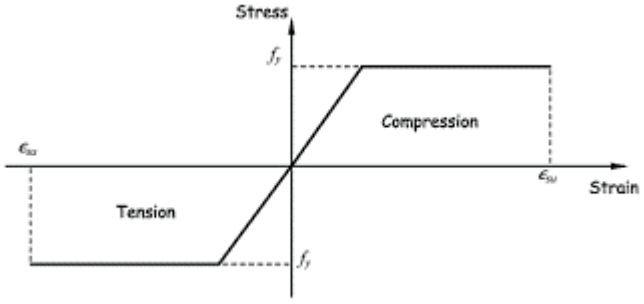

Fig. 6. Stress-strain model for steel in tension and compression.

3.5 Reinforcement modelling

Different mechanisms can be used to model the steel bars within a concrete element. Discrete modelling schemes were adopted where the link element for the steel reinforcing bar was connected between nodes of each adjacent concrete solid element, so the two materials share the same nodes, see Fig. 7. This algorithm will provide a full interaction between steel bars and concrete [20,11].

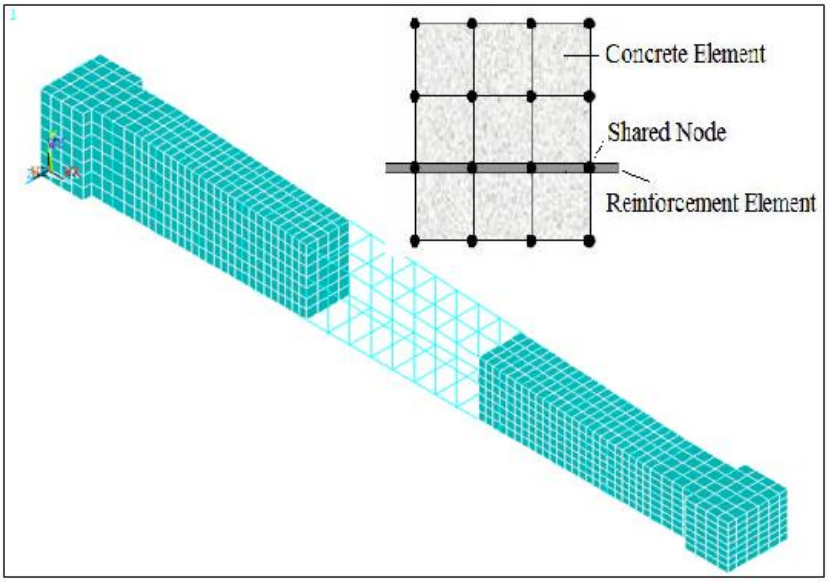

Fig. 7. Reinforcement layout.

3.6 Discretization

A Full section of a non-prismatic beam was considered and modelled. The mesh size was chosen in order to ensure the accuracy and geometry requirements. 20 mm mesh size was chosen in all directions, while this size changes along the taper edge according to the beam depth. Details of the specimen were shown in Fig. 8.

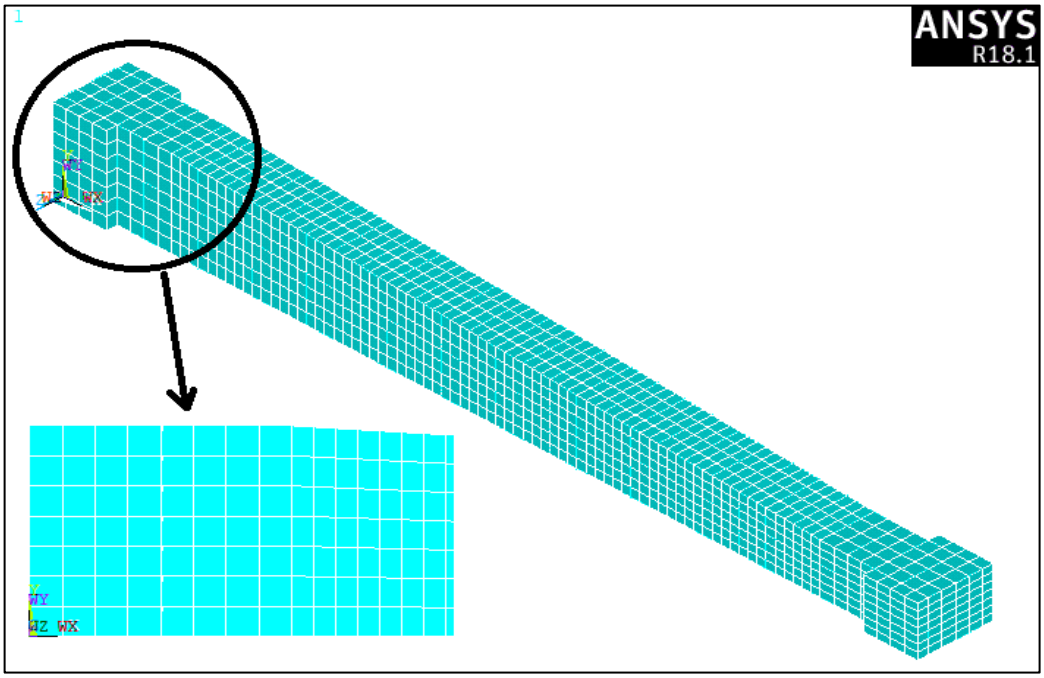

Fig. 8. Element discretization.

The difference in the results was minimal when the number of elements increased from 25000 to 30000 as shown in Fig. 9. Therefore, the 25000 elements model was selected for the modelling of beams with full reinforcements.

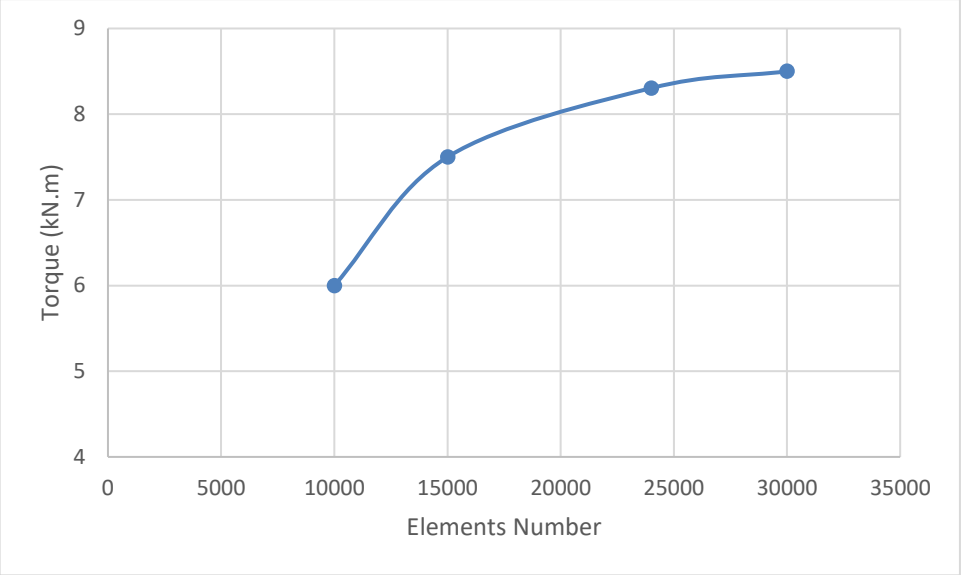

Fig. 9. Mesh density effect.

4. Experimental results and analysis

The non-prismatic beams were tested. The torsional moment and relative twisting angle are recorded and listed in Table 3. The important results collected which is, cracking torque (T_{cr}), cracking angle (θ_{cr}), maximum torque (T_{max}) and maximum angle (θ_{max}).

Table 3. Experimental results of non-prismatic beams.

Beam No.	Cracking torque T_{cr} *(kN.m)*	Cracking angle θ_{cr} *(rad)*	Max. Torque T_{max} *(kN.m)*	Max. Angle θ_{max} *(rad)*
B300-8-L	3.02	0.00566	9.76	0.043
B300-8	1.7	0.00225	7.59	0.0455
B300-10-L	4.89	0.0056	15.16	0.0457
B300-10	2.53	0.00202	12.588	0.0547
B225-8-L	2.56	0.00425	9.024	0.04457
B225-8	2.27	0.00625	7.01	0.0578
B225-10-L	2.98	0.0034	13.19	0.0445
B225-10	3.58	0.00451	11.21	0.0578

For the results listed in Table 3, it can be noted clearly that the presence of longitudinal torsional bars improves the torsional strength at pre and post-cracking stages. The location of these bars at mid-depth of beams improves the strength of concrete cover and hence gives more resistance to spalling and then torsional capacity due to strut action [21, 22]. This improvement was noted to be proportional to the steel reinforcement area. Moreover, its noted that the increase in tapering angle increases the strength of the non-prismatic beams. This is due to an increase in cross-sectional area that increases the torsional strength of beams. The overall experimental and numerical response of the tested specimens will be discussed in the present section.

4.1 Finite elements results and verification

The accuracy of the finite element model is examined by analysing a reinforced concrete non-prismatic beam subjected to pure torsion for which experimental results exist. The total response, cracking torque and ultimate torque value are compared with experimental data.

4.2 Torque- twist curve

Torque-twist curve of experimental and finite element data for the beam B300-8 tested under pure torsion is explained in Fig. 10. The curves match well in pre-crack and post-crack stages and diverge at ultimate load. It is noted clearly that experimental curve passes through three zones: linear, transition and yield zones. The linear zone represents the pre-cracking stage or elastic response of the beam. Transition zone represents the post-cracking stage where the load transmitted from concrete to steel reinforcement, while the yield zone represents the failure stage after steel yields.

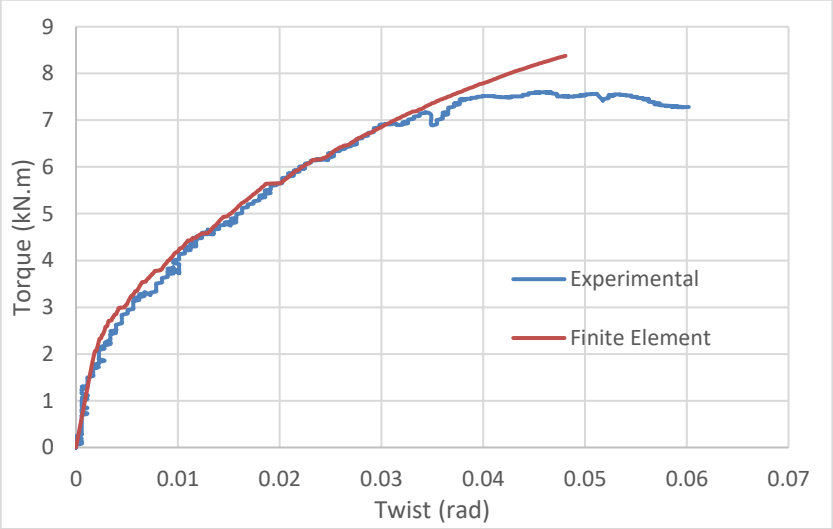

Fig. 10. Torque-twist curve of specimen B300-8.

Increasing the area of transverse reinforcement modify the strength of the beam as shown in Fig. 11 and the response is passes also through the three zones. These zones were conducted also through the response of prismatic beams under pure torsion [22].

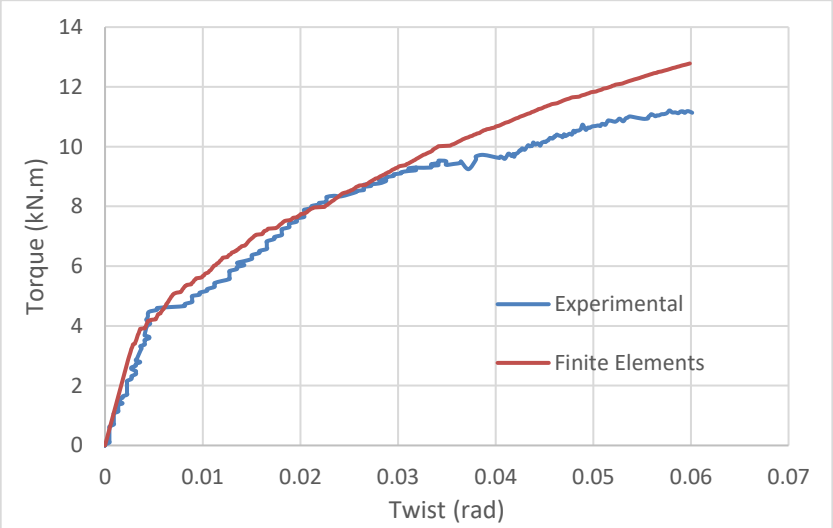

Fig. 11. Torque-twist curve of specimen B300-10.

The curve agrees well with the experimental data up to the ultimate load with a slight disagreement at this point.

Generally, the FE data looks to be stiffer than the experimental data due to the homogeneity and a full interaction assumption between concrete and steel reinforcement.

For specimens with smaller taper angle, the experimental torque-twist curves pass also through three stages as noted for specimens with higher taper angle. For specimen B225-8-L, the finite element model can predict accurately the response of these non-prismatic beams and describe this response from initial loading to ultimate load as explained in Fig.12

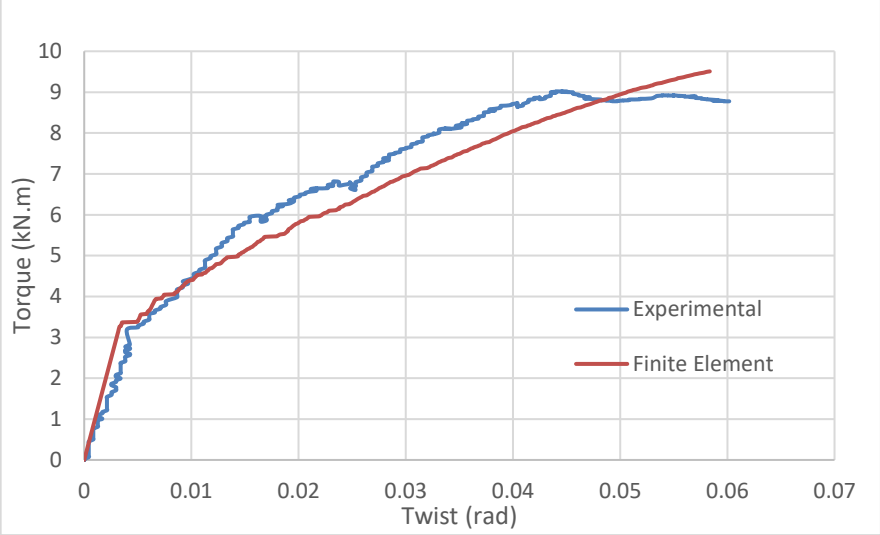

Fig. 12. Torque-twist curve of specimen B225-8-L beam.

Transition zone was noted to be larger than other zones (elastic and yield zones) in comparison to higher taper angle. This may be attributed to the decrease in torsional strength and the drop in torsional stiffness of the specimen.

The trend was detected also when steel reinforcement ratio was changed as shown in Fig. 13 for beam B225-10-L. The mismatch between experimental and numerical data was attributed also to the homogenous assumption of finite element model. Moreover, the divergence at maximum torque may be due to the assumption of full interaction between steel bars and concrete especially at advanced loading stages.

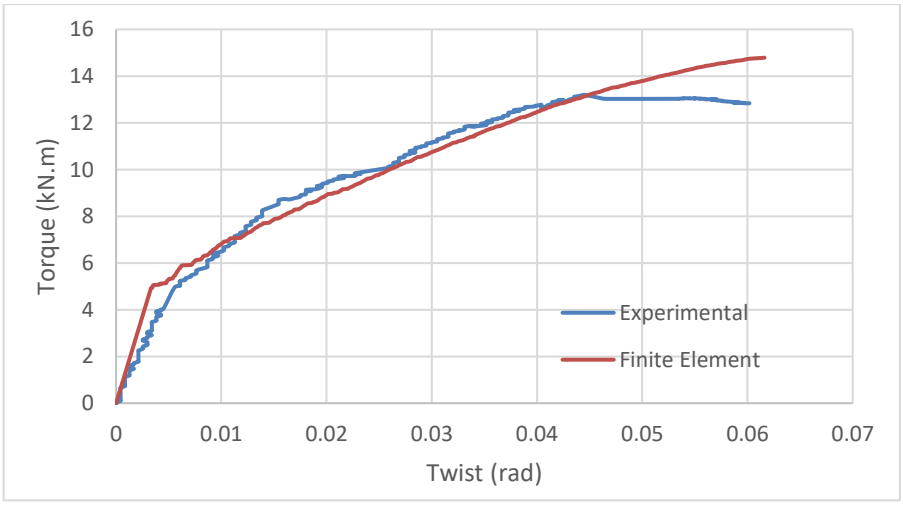

Fig. 13. Torque-twist curve of B225-10-L beam.

Generally, the comparison between experimental and FE data was listed in Table 4 for cracking torque and in Table 5 for maximum torque values in addition to its related twisting angle. It can be noted that the cracking torque detected by FE diverged about the experimental data. The value of standard deviation calculated for the diverge in cracking load value (16.1) displays the disagreement value in the result. This is can attributed mainly to the sensitive nature of cracks in experimental specimens and to the many factors affecting the microcracks generation such as gravel interlock, shrinkage, specimen translating ... etc. For the values of maximum torque calculated by FE, Table 5, the standard deviation of (3.7) refer to good agreement with experimental data.

Table 4. Experimental and FE results of cracking torque.

Beam No.	Experimental		Finite Elements		Error (%)
	Cracking torque T_{cr} (kN.m)	Cracking angle θ_{cr} (rad)	Cracking. Torque T_{cr} (kN.m)	Cracking Angle θ_{cr} (rad)	
B300-8mm-T	3.02	0.00566	2.785	0.00219	-8.4
B300-8mm	1.7	0.00225	2.246	0.00221	24.3
B300-10mm-T	4.89	0.0056	4.97	0.0036	1.6
B300-10mm	2.53	0.00202	3.922	0.0041	35.4
B225-8mm-T	2.56	0.00425	3.28	0.0034	21.9
B225-8mm	2.27	0.00625	2.69	0.0029	15.6
B225-10mm-T	2.98	0.0034	4.95	0.00344	39.7
B225-10mm	3.58	0.00451	4.122	0.00317	13.1
Standard Dev.					16.1

However, the maximum torque value collected by FE shows a good agreement with experimental data as listed in Table 4. Limited mismatch can be attributed to the homogeneity assumed in FE model in addition to the full interaction assumed between steel bars and concrete.

Table 5. Experimental and FE results of maximum torque.

Beam No.	Experimental		Finite Elements		Error (%)
	Max torque Tmax (kN.m)	Max angle θmax (rad)	Max. Torque Tmax (kN.m)	Max. Angle θmax (rad)	
B300-8mm-T	9.76	0.043	10.699	0.0491	8.7
B300-8mm	7.59	0.0455	8.376	0.0481	9.4
B300-10mm-T	15.16	0.0457	17.4	0.066	12.8
B300-10mm	12.59	0.547	12.78	0.06	1.5
B225-8mm-T	9.02	0.04457	9.51	0.0586	5.1
B225-8mm	7.01	0.0578	7.87	0.0572	10.9
B225-10mm-T	13.19	0.0445	14.78	0.0616	10.7
B225-10mm	11.21	0.0578	11.91	0.0546	5.8
Standard Dev.					3.7

4.3 Cracking pattern and failure

All the specimens were tested under static loading to maximum torque and then failure. Its noted that small section side is more vulnerable to loading effect as shown in Fig. 14 for specimen B300-8-L. This means that the design of transverse reinforcement spacing adopted by ACI Code did not changes greatly the failure shape of non-prismatic beams.

Fig. 14. Crack patterns of beam B300-8-L.

The strength of smaller beams (B225-8-L) shows same behavior and the cover looks to be stiff and not spalled at ultimate load as shown in Fig. 15

Fig. 15. Crack patterns of beam B225-8-L.

Acknowledgment

The authors would like to express their sincere gratitude to the College of Engineering, Tikrit University, for providing the facilities and technical support that enabled this research. Special thanks are also extended to the Structural Engineering Laboratory staff for their assistance during the experimental work.

5. Conclusions

Experimental and numerical behaviour of a non-prismatic concrete beam under pure torsion is presented. The main conclusions that can be drawn from the study are:

•The maximum torsion value is proportional to the tapering angle.

•Adding longitudinal torsional reinforcement improves the torsional strength of the beam for different tapering angles.

•A finite element model can predict accurately the general response of the non-prismatic beams.

•The model verified can be extended to investigate the effect of non-prismatic beams with different parameters.

References

[1] T. Shuo, K. Okubo, J. Niwa, "The shear behavior of RC tapered short beams with stirrups", *J. Adv. Concr. Technol.*, vol. 17, pp.506–517, 2019.

[2] H. M. Albegmprli, M. Eren Güls ¸A. Cevik, “Comprehensive experimental investigation on mechanical behavior for types of reinforced concrete Haunched beam”, *Adv. Concr. Constr.*, vol. 7, no. 1, pp.39–50, 2019.

[3] C. Hou, T. Nakamura, T. Iwanaga, J. Niwa, “Shear behavior of rein- forced concrete and prestressed concrete tapered beams without stirrups”, *J. Jpn. Soc. Civ. Eng.*, vol. 5, pp.170–189, 2017.

[4] A. Tena-Colunga, H. I. Archundia-Aranda, O. M. González-Cuevas, "Behavior of reinforced concrete haunched beams subjected to static shear loading", *Eng. Struct.*, Vol. 30, no. 2, pp. 478-492, 2008.

[5] A. H. A. Al-Ahmed, A. H. Al-Zuhairi, A. M. Hassan, “Behavior of Reinforced Concrete Tapered Beams”, *STRUCTURES*, vol. 37, pp. 1098–1118, 2022.

[6] M. Qissab, M. M. Salman, "Shear strength of non- prismatic steel fiber reinforced concrete beams without stirrups", *Struct. Eng. Mech.*, vol. 67, pp. 347-358, 2018.

[7] H. B. Rauf, Y. A. Ramadhan, “Effect of size factor and tapered angles on the shear behavior and strength of haunched beams reinforced with basalt fiber reinforced polymer rebars: Experimental and analytical study”, *STRUCTURES*, vol. 61, 2024.

[8] H. B. Rauf, Y. A. Ramadhan, “Shear behavior and capacity of reinforced concrete haunched beams: comprehensive review, comparative analysis, and structural judgment”, *STRUCTURES*, vol. 57, 2023.

[9] H. B. Rauf, Y. A. Ramadhan, “Shear strength of reinforced concrete tapered beams by using systematic multiscale models and artificial neural network”, *Iran. J. Sci. Technol. Trans. Civil. Eng.*, vol. 13, no. 1, 2023.

[10] H. M. R Karrar, H. A. Numan, “Behavior of non-prismatic reinforced concrete beams: A review”, The 2nd International Conference of Engineering Science (CESC), May 2024.

[11] E. A. Godínez-Domínguez, A. Tena-Colunga, G. Juarcz-Luna, “Nonlinear finite element modeling of reinforced concrete haunched beams designed to develop a shear failure”, *Eng. Struct*, Vol. 105, PP 99-122, 2015.

[12] A. A. Jaafer A. W. Abdulghani, “Nonlinear finite element analysis for reinforced concrete haunched beams with opening”, International Conference on Materials Engineering and Science, vol. 454, 8 August 2018, Istanbul, Turkey.

[13] H. S. Jebur, “Nonlinear Finite Element Analysis of Reinforced and Plain Concrete Hunched Beams Under Torsion”, *CIV ENG ENVIRON SYST*, Vol. 17, no. 1, pp. 229-241, 2021.

[14] ACI Committee 318 (2019), Building code requirements for structural concrete and Commentary, American Concrete Institute, Farmington Hills, MI, USA.

[15] A. H. Nilson, D. Darwin, C. W. Dolan, Design of Concrete Structures, New York, USA, McGraw-Hill Companies, 2010.

[16] A. M. Neville, Properties of Concrete, Harlow, England, 5th ed., Pearson Education Limited, Prentice Hall, 2012.

[17] ASTM A615/615M-14, (2014). Standard Specification for Deformed and Plain Carbon-Steel Bars for Concrete Reinforcement, West Conshohocken, PA: ASTM International.

[18] ANSYS Program. ANSYS Manual help. Version 18.1, 2018.

[19] D. Kachlakev, T. Miller, “Finite element modeling of reinforced concrete structures strengthened with FRP laminates”, SPR 316, Oregon Department of Transportation Research Group & Federal Highway Administration, Washington DC, 2001.

[20] A. J. Wolanski, "Flexural Behavior of Reinforced and Prestressed Concrete Beams Using Finite Element Analysis", Master's Theses, Marquette Campus, 2004.

[21] C. E. Chalioris, “Experimental study of the torsion of reinforced concrete members” *Struct. Eng. Mech.*, vol. 23, no. 6, pp. 713-737, 2006.

[22] L.F.A. Bernardo, S.M.R. Lopes, “Theoretical behavior of HSC sections under torsion”, *Eng. Struct*, vol. 33, no. 12, PP. 3702-3714, 2012.